Supplementary Information

Convergent evolution of a genomic rearrangement may explain cancer resistance in hystrico- and sciuromorpha rodents

Yachna Jain[1], Keerthivasan Raanin Chandradoss[1], Anjoom AV[1], Jui Bhattacharya, Mohan Lal, Meenakshi Bagadia, Harpreet Singh, Kuljeet Singh Sandhu[*]

Department of Biological Sciences
Indian Institute of Science Education and Research (IISER) – Mohali
Knowledge City, Sector 81, SAS Nagar 140306, Punjab, India.

[1]Equal contribution
[*]Correspondence to sandhuks@iisermohali.ac.in

Supplementary Table 1. Details of the datasets used in the study

Analysis	Data-type / tool	Species	Tissue	Database	Accession / link
Gene expression	RNA-Seq	human	Thymus	GEO ENCODE	GSM2935638
			Skin		ENCFF549LHP
			Ovary		ENCFF479CKA
			Kidney		ENCFF251XMZ
			Adrenal		ENCFF480JAT
			Heart		ENCFF205LNA
			Testis		ENCFF662BIH
			Liver		ENCFF039WAC
		mouse	Skin		GSM1606093
			Thymus		ENCFF074ZUD
			Ovary		ENCFF097YQV
			Kidney		ENCFF167GTO
			Adrenal		ENCFF916CFV
			Heart		ENCFF456GZP
			Testis		ENCFF456PSH
			Liver		ENCFF880OSE
		NMR	Skin		GSE98719
			Thymus		
			Ovary		
			Kidney		
			Adrenal		
			Heart		
			Testis		
			Liver		
		Guinea pig	Skin		
			Thymus		
			Ovary		
			Kidney		
			Adrenal		
			Heart		
			Testis		
			Liver		
	Array	Woodchuck	Liver, Spleen, Kidney		GPL15354
Spatial proximity	Hi-C	Human	Aorta	PennState Hi-C browser	Leung et al (2015) Schmitt et al (2016)
			Liver		
			Adrenal		
			Bladder		
			Psoas		
			Pancreas		
			Spleen		
		Mouse	Liver	GEO	GSE58752 GSE65126
		Monkey			
		Dog			
		Rabbit			

		NMR	Embryonic fibroblasts	SRA	SRR8204318
Chromatin accessibility	ATAC-Seq	NMR	Skin fibroblast	GEO	GSE83585
	DNase-Seq	Human	Body of pancreas	ENCODE	ENCFF095KFF
			Breast epithelium		ENCFF322ALX
			Upper lobe of left lung		ENCFF414NAA
			Tibial artery		ENCFF367MHB
			Gastrocnemius medialis		ENCFF082TEM
			Ovary		ENCFF338CIA
			Thyroid gland		ENCFF126DFR
			Esophagus muscularis mucosa		ENCFF951HWM
			Coronary artery		ENCFF871GME
			Prostate gland		ENCFF069GRI
			Stomach		ENCFF922TBR
			Small intestine		ENCFF619LIB
			Lower leg skin		ENCFF561DJM
			Pancreas		ENCFF230OUF
			Omental fat pad		ENCFF037ZSW
			Tibial nerve		ENCFF094FZF
			Esophagus squamous epithelium		ENCFF376RIO
			Ascending aorta		ENCFF233ORX
			Vagina		ENCFF154NSS
			Transverse colon		ENCFF413EKZ
			Sigmoid colon		ENCFF410TTD
			Right lobe of liver		ENCFF462ZLK
			Spleen		ENCFF047HXB
			Uterus		ENCFF037DUA
			Testis		ENCFF068YUS
			Heart left ventricle		ENCFF678EIG
			Adrenal gland		ENCFF150WZO
			Frontal cortex		ENCFF110QGM
			Globus pallidus		ENCFF225FYX
			Pons		ENCFF210SQU
			Midbrain		ENCFF547ZQF
			Heart		ENCFF303XQF
			Cerebellar cortex		ENCFF564DYF
			Putamen		ENCFF681JFJ
			Psoas muscle		ENCFF846FZJ
			Inferior parietal cortex		ENCFF848BGL
			Occipital lobe		ENCFF568EAH
			Superior temporal gyrus		ENCFF029ZOX

			Medulla oblongata		ENCFF151SBP
			Middle frontal gyrus		ENCFF751LHL
			Caudate nucleus		ENCFF498QFP
		Mouse	Lung		ENCFF043UNG
			Forelimb bud		ENCFF837OUY
			Hindbrain		ENCFF943PHW
			Limb		ENCFF641OPE
			Brain		ENCFF992QCB
			Forebrain		ENCFF684BQC
			Embryo		ENCFF627IDE
			Retina		ENCFF908NIP
			Neural tube		ENCFF649UQO
			Embryonic facial prominence		ENCFF311WRA
			Liver		ENCFF395XSI
			Midbrain		ENCFF942RUO
			Heart		ENCFF773NKY
			Kidney		ENCFF299KAN
			Hindlimb bud		ENCFF037VPV
			stomach		ENCFF773UVA
			Thymus		ENCFF125IRZ
			Gonadal fat pad		ENCFF090NJT
			Large intestine		ENCFF650OFZ
			Yolk sac		ENCFF353HPD
			Cerebellum		ENCFF474GND
			Intestine		ENCFF424BHU
			Spleen		ENCFF546FZT
			Telencephalon		ENCFF238ZRM
			Fat pad		ENCFF243REK
			Mesoderm		ENCFF673VVB
			Skeletal muscle tissue		ENCFF731YAA
TSGs & POGs		Human		CancerMine	http://bionlp.bcgsc.ca/cancermine/
GC content		NMR		UCSC	https://genome.ucsc.edu/
Linkage disequilibrium		Human		Broad Institute FTP server	http://homer.ucsd.edu/homer/interactions/
Lamin-B1 enrichment	ChIP-Seq	Mouse	ESC	GEO	GSE17051
Replication timing	Repli-chip	Human	GM06990	ENCODE	https://hgdownload-test.gi.ucsc.edu/goldenPath/hg19/encodeDCC/wgEncodeFsuRepliChip/release1/
			H9ES		
			Hela		
			IMR90		
		Mouse	CH12		http://hgdownload.cse.ucsc.edu/goldenpath/mm9/encodeDCC/wgEncodeFsuRepliChip/
			EPISC		
			ESC		
			L1210F		
			MEFM		
			MEL		

UV transmission	50% T	38 mammals	Eye lens		Douglas and Jeffery (2014). https://doi.org/10.1098/rspb.2013.2995
Recombination rates		Human and mouse		-	Jensen-Seaman et al, 2004
Temporal activity data		>4000 species		AnAge	https://genomics.senescence.info/species/stats.php
Hi-C processing	SRA Toolkit				https://www.ncbi.nlm.nih.gov/sra/docs/toolkitsoft/
	HiCUP				https://www.bioinformatics.babraham.ac.uk/projects/hicup/
	Homer				http://homer.ucsd.edu/homer/interactions/
	PennState Hi-C browser				http://promoter.bx.psu.edu/hi-c/
CNVs, gene expression across cancers	Xena browser	Human			https://xenabrowser.net/
Orthologous chr/scaffold coordinates	UCSC Liftover				https://genome.ucsc.edu/cgi-bin/hgLiftOver
Gene ontology	ToppGene suite				https://toppgene.cchmc.org/
Genome browsers	UCSC genome browser				https://genome.ucsc.edu/
	Ensembl genome browser				https://asia.ensembl.org/index.html
Analysis of body mass and max. longevity	TimeTree	Myomorpha, Hystricomorpha & Sciuromorpha			http://www.timetree.org/
	Phytools				http://www.phytools.org/eqg2015/asr.html
	AnAge database				https://genomics.senescence.info/species/
Statistics	R				https://www.r-project.org/
Visualization	ggplot2				https://ggplot2.tidyverse.org/

Supplementary Table 2. Distances between NME6 and PLXNB1 genes in genomes of human, myomorphs, sciuromorphs and hystricomorphs. In hystricomorphs, the genes were present in different scaffolds. To calculate the NME6-PLXNB1 distances, the scaffolds were joined in all possible orientations (1 convergent, 1 divergent and 2 tandem orientations), and the smallest distance of all combinations (the worst case scenario) was considered.

Species	Chr/Scaffold	Plxnb1-Nme6 distance (Mb)	Chr/Scaffold	Nme6-Camp distance (Mb)
Human	Chr3	0.113132	Chr3	0.067375
Myomorphs				
Mouse	Chr9	0.73736	Chr9	0.014630
Rat	Chr8	0.084243	Chr8	0.009602
Mongolian gerbil	NHTI01000042.1	0.08431	NHTI01000042.1	0.010237
Golden hamster	KB708177.1	0.095007	KB708177.1	0.014740
Blind mole rat	KL204508.1	0.537969	KL204508.1	0.044576
Kangaroo rat	KN672453.1	0.045737	KN672453.1	0.005384
Sciuromorphs				**Min. of all orientations**
Squirrel	JH393339.1	0.111261	Different scaffolds	1.800195
Alpine Marmot	CZRN01000020.1	0.146779	Different scaffolds	8.122866
Arctic ground squirrel	Different scaffolds	0.155398	Different scaffolds	2.557477
Daurian squirrel	PLXNB1 ortholog not found		Different scaffolds	0.388004
Hystricomorphs				
NMR	JH602043.1 (hetGla2 assembly)	71.045	JH602043.1	0.015136
	RPGA1000013.1(GCA_014060925.1 assembly)	78.407	RPGA1000013.1(GCA_014060925.1 assembly)	0.015071
Other hystricomorphs		**Min. of all orientations**		
Chinchilla	Different scaffolds	6.413811	CAMP Ortholog not found	
Brazillian guinea pig	Different scaffolds	36.147762	AVPZ01000778.1	0.014144
Damara mole rat	Different scaffolds	5.109729	KN122104.1	0.011282
Degu	Different scaffolds	2.284109	Different scaffolds	2.175631
North American porcupine	Different scaffolds	1.281664	ML655359.1	0.010105
Domestic guinea pig	Different scaffolds	36.149925	DS562862.1	0.015158

Supplementary Table 3. List of genes, located in 3p21-22 (sea green), 3q (red), 19p13.11 (orange), and other (black) loci, that are associated with evolutionarily diverged traits in hystrico- and sciuromorphs

Function	Genes	Cytoband	Role
Negative regulation of growth	SEMA3F,HYAL1,CCR2, SEMA3B,NME6,HYAL 2,IP6K2, SETD2	3p21.31	Growth and tumour suppression
UV response	HYAL1, HYAL2, HYAL3, TMEM161A	3p21.31, 19p13.11	Cancer, UV-response, vision, skin elasticity
Hyaluronan binding	HAPLN4, NCAN	19p13.11	hibernation
Inflammatory response	XCR1,TREX1,IMPDH2, HYAL1,CCR9,TRAIP,T DGF1,CCR2,MST1R,H YAL3,CCR1,CCR3,SLC 26A6,HYAL2,IP6K2	3p21.31	Cancer, wound healing
DNA metabolism	EREG,AREG,CXCL8,PA RM1	4q13 (NMR-4)	Genome maintenance
Thermoregulation	PTH1R	3p21.31	Poikilothermism, hibernation
Hypoxia tolerance	UQCRC1	3p21.31	Sub-terranean habitat, hibernation
Vitamin-A metabolism	GRM2, RBP1, RBP2	3p21.2, 3q23	Vision, hibernation,
Enamel mineralization	ENAM, AMTN	20p13(GP-2)	Grinding
Mating behaviour	OXT,AVP,	3q(GP-1)	Diverse mating behaviour
Amino Acid metabolism	GLYCTK, ALAS1, GRM2	3p21.2	hibernation
Regulation of telomere maintenance	PARP3, CERS1, XRN1, ATR, STAG1, CEP63	3p21.2, 19p13.11, 3q	Aging, cancer-resistance
Atrial blood pressure	MANF	3p21.2	Hibernation
Regulation of kinase activity	CISH, DUSP7, MAPKAPK3, BORCS8, MEF2B, DOCK3	3p21.2,19p13.11	Hibernation
Blood coagulation	FGA,FGB,FGG	4q28(GP-3)	Wound healing
Lipid homeostasis	SCAP, ACAD11, TM6SF2, PLSCR gene-family, ESYT3, SLCO2A1, AGTR1,	3q22/23, 19p13.11, 3p21.31, 3p22	Hibernation
Calmodulin binding	IQCF1, IQCF2, IQCF3, IQCF4, IQCF5, IQCF6	3p21.2	Hibernation
Eye development	SOX2,PCYT1A, SCAP, DHX30, CDC25A	3q(NMR-5), 3p21.31	Vision
Matrix (other than HA related)	COL6A6, PCOLCE2, PLOD2, PLXNB1, CSPG5, CILP2	3q22.1, 3p21.31, 19p13.11	Wound healing, aging, cancer, skin etc.

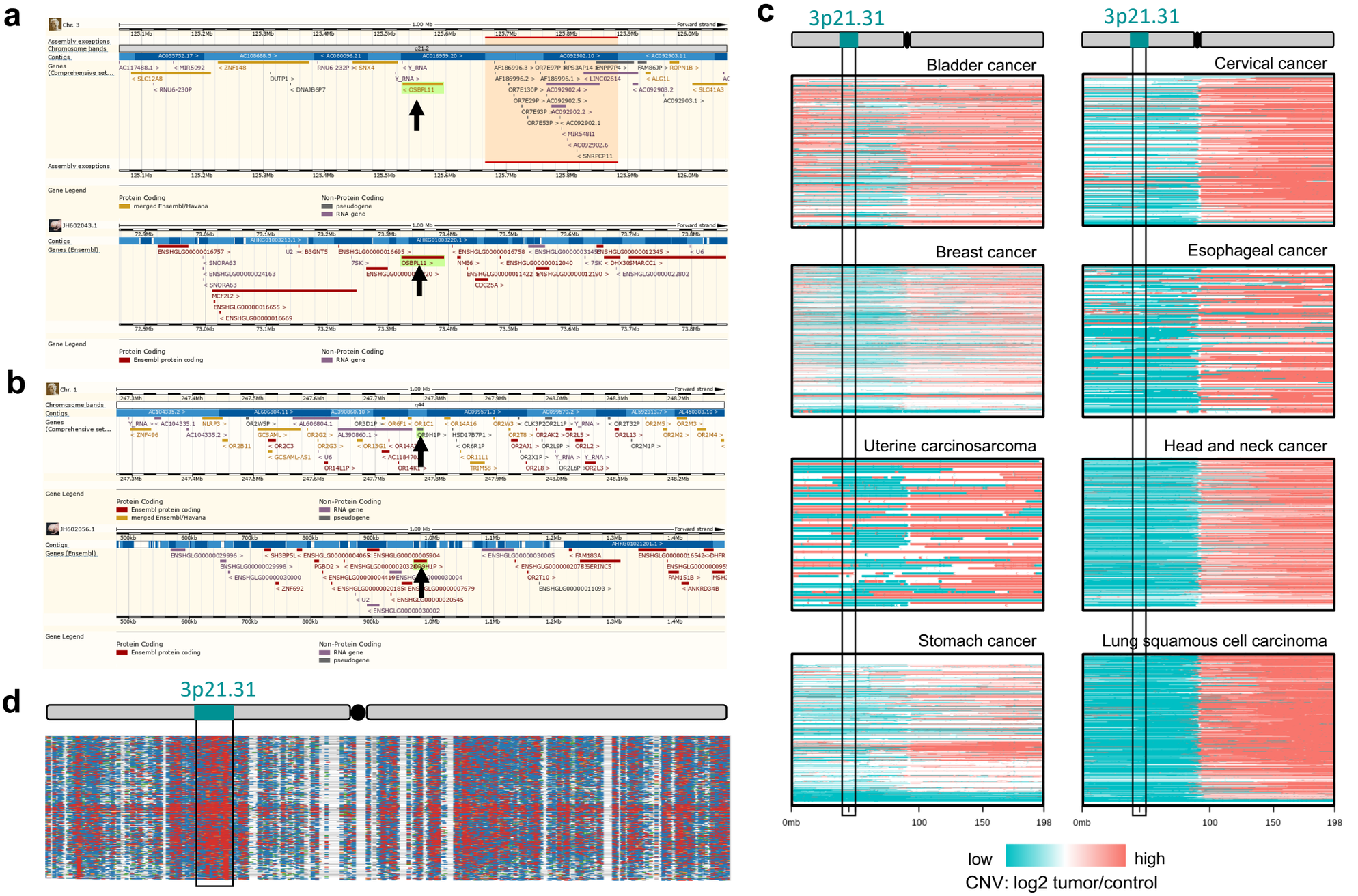

Supplementary Figure 1. (a-b) Single gene repositioning events between Human (top panel) and NMR (bottom panel). The OSBPL11 and OR9H1P genes are indicated by arrow-heads. Comparing the immediate neighbourhood of these genes in Human and NMR negates the possibility of translocation or inversion. OSBPL11 is adjacent to a region marked as “assembly exceptions” (highlighted in red), implying the possibility of erroneous sequence mapping. OR9H1P lacked introns and is annotated as pseudogene, hinting at differential retro-transposition of the gene in human and NMR. (c) Amplification and deletion of various chr3 regions across different cancers in human. (d) Frequency of somatic point mutations in TCGA cohort. Data was directly pulled down from UCSC Xena browser. Red: deleterious mutations; blue: missense mutations.

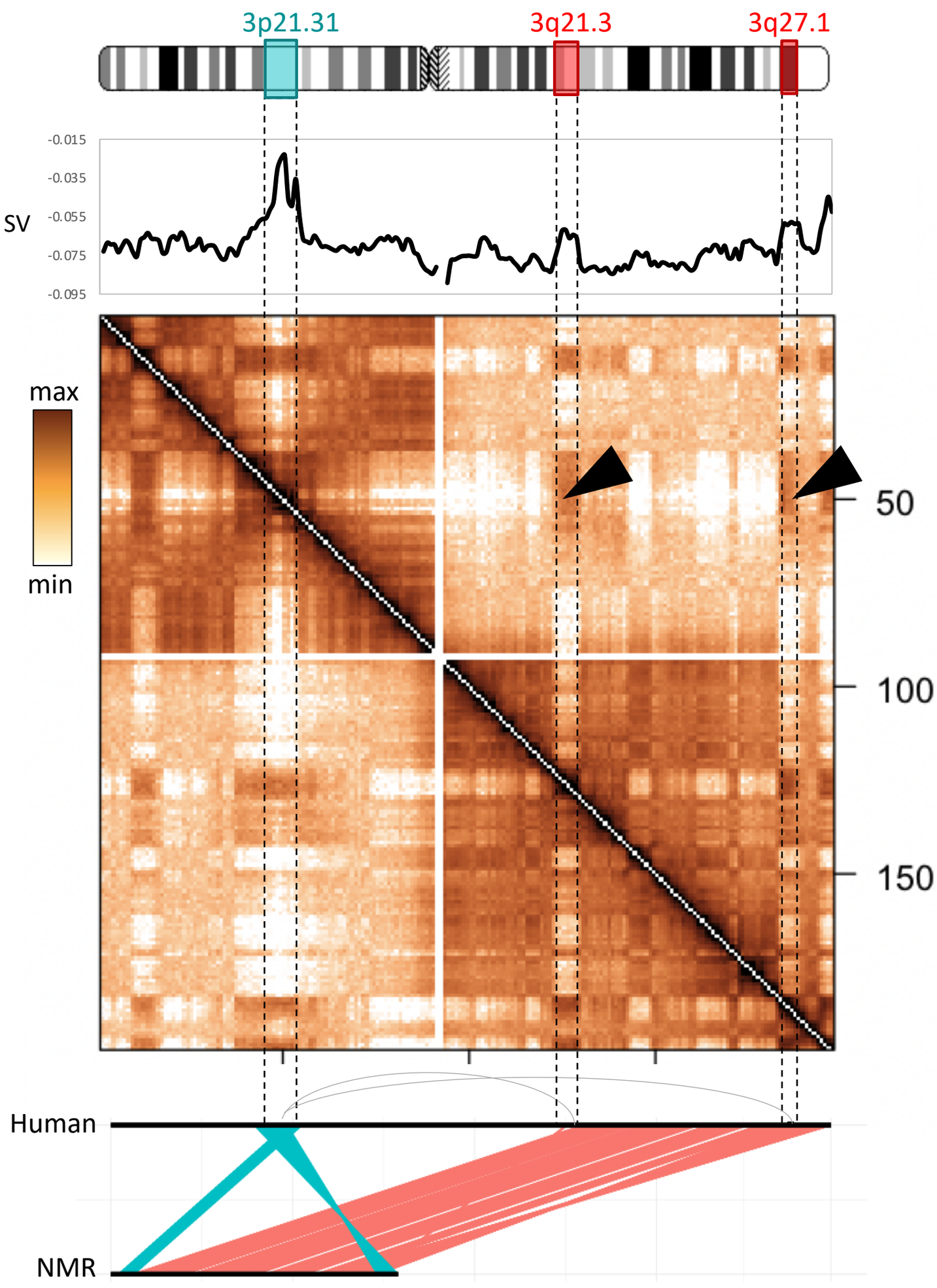

Supplementary Figure 2. Hi-C contact map of entire chr3 of human (liver, 1Mb resolution), aligned onto the map of human-NMR genomic rearrangement. The top panel shows chr-3 ideogram followed by the leading singular vector of normalized Hi-C contact matrix. Arrow-heads highlight the regions that show high frequency of contacts with 3p21.31 locus. These regions coincide with the human-NMR breakpoints on 3q arm.